Electronic State of Oxidized Nanographene Edge with Atomically Sharp Zigzag Boundaries

Misako Ohtsuka, Shintaro Fujii,* Manabu Kiguchi, and Toshiaki Enoki*

Department of Chemistry, Tokyo Institute of Technology, 2-12-1 Ookayama, Meguro-ku, Tokyo 152-8551, Japan

ABSTRACT Combined scanning tunneling microscopy (STM) and density functional theory (DFT) characterizations of the electronic state were performed on the zigzag edge of oxidized nanographene samples. The oxidized zigzag edge with atomically sharp boundaries was prepared by electrochemical oxidation of the graphite surface in aqueous sulfuric acid solution. Bias-dependent STM measurements demonstrated the presence of the edge state at the zigzag edges with local density of states (LDOS) split into two peaks around the Fermi level. Our DFT-based analysis showed that the two-peak structure of the edge state was due to the termination of the zigzag edge by carbonyl functional groups. The LDOS arising from the edge states was slowly dampened in the bulk at the carbonyl-terminated zigzag edges (~1.5 nm). This result is in clear contrast to the strongly localized edge states at hydrogenated zigzag edges in previous reports. The oxygen atoms in the carbonyl functional groups act as additional π sites at the edges; thus, the topology of the π electron network changes from "zigzag" to "Klein" type, leading to drastic modification of the edge states at the oxidized edges.

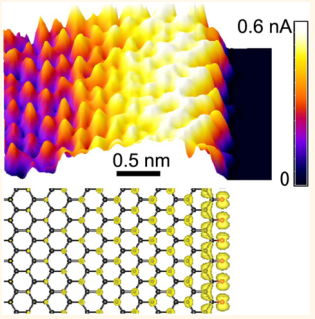

KEYWORDS: graphene · oxidation · electronic structure · scanning tunneling microscopy · density functional theory

Graphene, a single atomic layer of graphite, has attracted considerable interest because of its unique electronic properties.[1,2] These properties arise from its electronic structure near the Fermi level. Because of the biparticity of the two-dimensional honeycomb π electron network, graphene has zero gap at the Dirac point with linear dispersion relation, and its electron motion near the Dirac point is effectively described by the relativistic Dirac-type equation rather than by the Schrödinger equation.[3] Interestingly, the unique electronic properties of graphene can be modified by introducing boundaries (*i.e.*, edges) in the infinite π electron network.[4−7] The edge geometry is described by a combination of the two typical crystallographic directions, that is, zigzag and armchair. The effect of edge geometries on the electronic properties of graphene has been theoretically investigated by the tight-binding approach of zigzag and armchair-terminated graphene nanoribbon (GNR) models, in which unconventional flat bands at the Fermi energy (E_f) are predicted to appear only at hydrogenated zigzag-shaped graphene edges.[8,9] Although pristine graphene is a zero-gap semiconductor with vanishing density of states (DOS) at E_f, the introduction of the zigzag edge induces the unique edge-localized π state at E_f, which is referred to as the edge state.[9] Recent progress in scanning probe microscopic techniques has allowed us to confirm experimentally the presence of the edge state at the hydrogenated zigzag edges.[10−15] Although most experimental research has focused on the edge state of the prototypical hydrogenated edge, promising future applications of the edge state to all-carbon-based electronic devices require controlled chemical modification of the zigzag edges; the chemical details at the zigzag edges have been predicted to significantly affect the band dispersion and spatial distribution of the edge state. In this context, a large number of theoretical studies have recently appeared in the literature.[16−22] For example, a previous theoretical study investigated the effect of oxidation on the edge state using hydroxyl-,[18,19] carbonyl-,[19−22] and ether-terminated[18,22] zigzag GNR models, in which the carbonyl termination induces non-negligible band dispersion to the original edge state flat bands.[18] However, experimental characterization remains a challenging task

* Address correspondence to fujii.s.af@m.titech.ac.jp, tenoki@chem.titech.ac.jp.

Received for review April 24, 2013 and accepted July 19, 2013.

Published online July 19, 2013
10.1021/nn402047a

because of difficulties in oxidizing graphene sheets in a controlled manner. In fact, chemical oxidation of graphene materials using $KMnO_4$ proceeds in a rather random manner, in which graphene planes are heavily modified by oxygen-containing functional groups such as hydroxyl and epoxide groups to form graphene oxide.[23] In the present study, electrochemical oxidation[24,25] of graphite surface edges was carried out to prepare oxidized graphene edges. In principle, edge-selective oxidation and control over the oxidation levels are possible by fine-tuning the electrochemical potential during the reactions. In the following, we start by presenting an electrochemical analysis of the graphite surface to investigate the electrochemical activity of graphite surface edges. We then focus on scanning tunneling microscopy (STM) characterization of the edge state appearing at the resultant electrochemically oxidized zigzag edges. Finally, we demonstrate that the chemical nature of the oxidized zigzag edges could be identified based on investigation of bias-dependent STM measurements and corresponding first-principles calculations.

RESULTS AND DISCUSSION

The anodic oxidation of the graphite surface was performed in a 0.1 M H_2SO_4 solution at room temperature. The oxidation potentials were 1.7, 1.8, and 1.9 V *vs* RHE (reversible hydrogen electrode). Figure 1 shows cyclic voltammograms of the graphite surface in dilute H_2SO_4 solution. The oxygen evolution on the graphite surface, which appeared as an exponential current in the voltammogram, increased as the potential became more positive. The oxygen evolution led to fragmentation of the graphite surface to form nanosized graphene fragments with electrochemically oxidized edges. *In situ* electrochemical STM measurement of the graphite surface in dilute H_2SO_4 solution under an electrochemical potential (0.3−0.8 V *vs* RHE) suggests that the electrochemical oxidation (*i.e.*, C−C bond breakages and CO_2 formation[26]) starts from the graphite surface edges, leading to fragmentation into nanosized fragments. Previous X-ray photoelectron spectroscopy (XPS) studies on electrochemically oxidized graphite surfaces in 0.5 M H_2SO_4 solution have demonstrated that hydroxyl, carbonyl, and carboxyl functional groups are formed on the surface after repeated potential cycling from 0.8 to 1.0 V (*vs* SHE (standard hydrogen elelectrode)) with sweep rates of 10 and 90 mV s^{-1}.[26] To investigate the atomic-scale fragmentation process during the heterogeneous oxygen evolution on the surface studied here, further future studies of *in situ* electrochemical STM measurements will be required.

Figure 2 shows STM topographic images of the graphite surface after 10 cycles of a potential sweep from 1.0 to 1.9 V (Figure 1c), in which significant fragmentation of the graphite surface was apparent. Atomically resolved STM topographic imaging of the

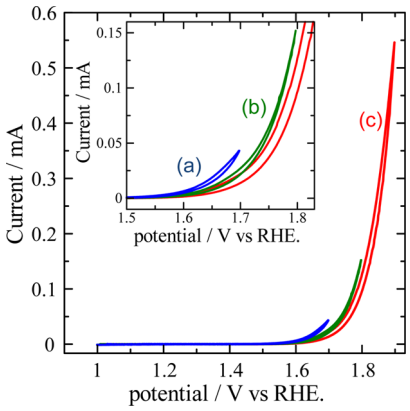

Figure 1. Cyclic voltammetric profiles of graphite surface in 0.1 M H_2SO_4 solution, taken at 20 mV s^{-1} in the potential ranges (a) 1.0−1.7 V, (b) 1.0−1.8 V, and (c) 1.0−1.9 V. Inset: magnified images of the cyclic voltammogram for (a) and (b) are shown for clarity.

graphene fragments revealed that a large part of the honeycomb π electron network in the graphene plane was preserved after the oxidation (Figure 2c), while electronic structure at their edge boundaries was considerably altered on the atomic scale, which is due to variations in geometrical shape of the edges as well as chemistry of the edge terminations introduced by the rupture process of the graphene surface in the electrochemical oxidation (Figure 2b,d). The lateral size of the graphene fragments ranged from 20 to 100 nm, and the thickness consisted of one to four layers, as shown in Figure 3a,b. A closer examination of atomic-scale STM images of the nanographene edge boundaries revealed that not only ill-defined (ragged) edge boundaries (Figure 2d) but also atomically sharp edge boundaries terminated along a zigzag direction (Figure 4a) were present on the periphery of the nanographene fragments. The probability of finding such atomically smooth oxidized edges along the zigzag direction was less than 10%. The remaining edges were more likely to consist of a mixture of zigzag and armchair edges on the atomic scale (Figure 2d), where stable STM imaging with atomic resolution was hardly possible, which is mostly due to structural deformations induced by random attachments of oxygen-containing functional groups. The ragged edge boundaries could have originated from heterogeneous electrochemical oxidation at the atomically ill-defined graphene edges prepared by mechanical cleavage of the highly oriented pyrolytic graphite (HOPG) sample. A cross-sectional profile of the nanographene fragment with atomically smooth edges on the graphite substrate exhibited that the thickness of the nanographene fragment was 0.3−0.4 nm (Figure 4a), which corresponds to that of a single graphene sheet on a graphite surface (0.335 nm). Higher-magnification STM imaging at the zigzag boundaries in Figure 4b revealed that the edge state has an enhanced LDOS (*i.e.*, brighter bump) extended into the bulk at $a \times a$ periodicity (a = graphene lattice constant). It should be noted that most of

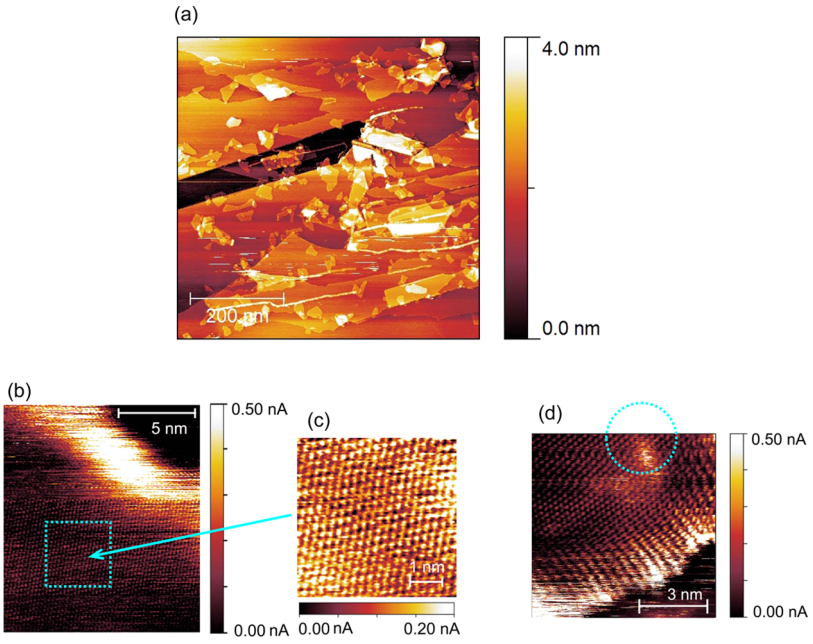

Figure 2. (a) STM topographic image of graphite surface after 10 cycles of a potential sweep from 1.0 to 1.9 V at 20 mV s^{-1} (see Figure 1c). Fragmentation of the graphite surface is apparent. Imaging conditions: tunneling current (I_t) = 0.4 nA, V_{bias} = 800 mV. (b,d) STM current images of nanographene edges. (c) Magnified image in a dotted square region in (b). Imaging conditions: V_{bias} = (b,c) 200 mV, (d) 500 mV. In (d), atomic size defect, possibly prepared by in-plane oxidation process during the electrochemical oxidation, is indicated by a dotted circle. The possibility of identifying such in-plane defects is less than 10%.

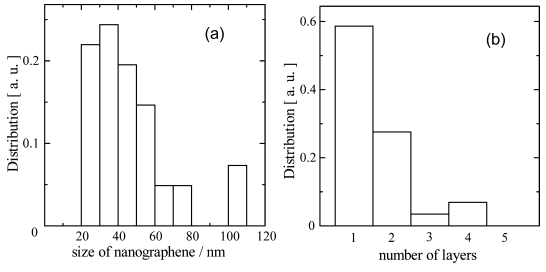

Figure 3. Histograms of size (a) and thickness (b) distribution of nanographene fragments prepared by electrochemical oxidation.

the nanographene fragments presented Bernal stacking order (A−B stacking) with respect to the graphite surface.[27,28] In contrast, relatively large nanographene fragments (>100 nm) occasionally displayed a random stacking order (higher order commensurate adlayer structure) with a moiré pattern (superstructure) of LDOS in the STM images.[27,28] The unique enhancement of the LDOS distribution at the zigzag boundaries (Figure 4c) could be identified by comparing it with that near the armchair boundaries in a nanographene fragment (Figure 4d), in which the LDOS distribution was almost constant over the nanographene fragment.

The delocalized character of the edge state decaying into the interior of graphene plane from the oxidized edges was in sharp contrast to the strongly localized edge state at the zigzag edges.[10−15] In our previous STM studies of hydrogenated zigzag edges,[10,15] the edge state was identified as bright spots (*i.e.*, enhanced LDOS)

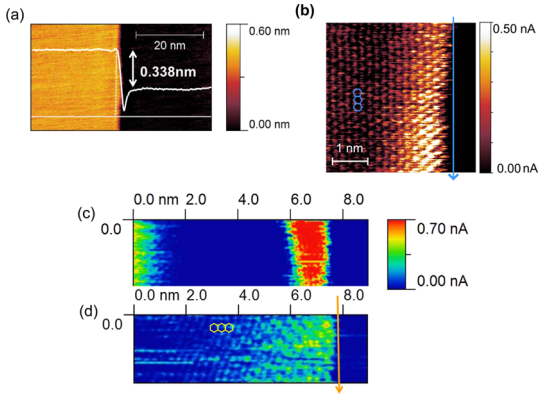

Figure 4. (a) STM topographic image of a nanographene fragment on a graphite substrate. A cross-sectional profile along the horizontal bold line is superimposed on the image (*z*-scale bar = 0.415 nm). Imaging conditions: I_t = 0.3 nA, V_{bias} = 730 mV. (b) High-resolution STM constant-height image of an oxidized zigzag edge of the nanographene fragment with Bernal stacking order on the graphite surface. Here, an atomically sharp edge boundary of several nanometers is apparent. Brighter dots (*i.e.*, edge state) represent large amplitudes on one of the graphene sublattice sites (β carbon) with $a \times a$ periodicity (a = 0.24 nm) that decay into the bulk from the edge boundary. A honeycomb pattern of the graphene lattice is superimposed on the image. The zigzag direction is denoted by an arrow. (c,d) High-resolution STM constant-height images of the zigzag (c) and armchair (d) edges of the nanographene fragments. (A honeycomb pattern of the graphene lattice is superimposed on the image. The zigzag and armchair directions are denoted by arrows in (c) and (d), respectively.) In contrast to the armchair edge, the zigzag edge features enhanced LDOS (*i.e.*, the edge state). Imaging conditions: (c) V_{bias} = 200 mV, (d) V_{bias} = 500 mV.

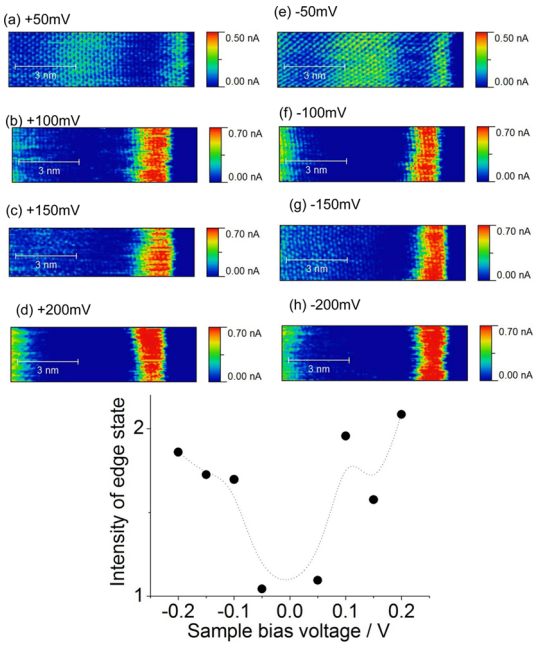

Figure 5. (a−h) Bias-dependent constant-height STM measurements on the oxidized zigzag edge (see Figure 4a). Imaging conditions: V_{bias} = (a) +50 mV, (b) +100 mV, (c) +150 mV, (d) +200 mV, (e) −50 mV, (f) −100 mV, (g) −150 mV, and (h) −200 mV. The intensity of the LDOS around the zigzag edge (*i.e.*, edge state) with respect to that of the LDOS on the interior carbon atoms (bulk state) was strongly dependent on V_{bias}. (i) Intensity of the edge state as a function of V_{bias} for bulk carbon wherein a quasi-gap structure is apparent. The intensity of the edge state was normalized with respect to the intensity of bulk graphene (interior plane carbon atoms). The dotted line is a visual guide. The STM intensity is largely subject to tip−sample distance as well as the bias voltage during the imaging. In our experimental setup, precise control of the tip−sample distance is hardly realizable. Therefore, the edge state intensity was normalized by that of the bulk state, which is an internal standard for STM intensity in each STM image.

localized at several atomic sites from the zigzag boundaries. In contrast, the edge state at the oxidized edges studied here featured an exceptionally wide distribution of bright spots up to 1.5 nm away from the edge boundaries. Such wide distribution of the bright spots (spatially extended character) may result from a topographic effect in folded edge structures.[29] However, this is not the case in the present study because the enhanced LDOS distribution around the zigzag edges is strongly subject to the bias voltage, V_{bias} (*i.e.*, purely electronic effect), as explained below.

Figure 5a−h shows a series of STM current mapping images taken at various values of V_{bias} (from −200 to +200 mV). At the lower bias voltage of ±50 mV, the edge state intensity was suppressed, while it became more pronounced as the bias increased. Such suppression of the edge state intensity cannot be realizable at the hydrogenated zigzag edges because the edge state at the hydrogenated edges has sharp DOS distribution around zero bias[8,9] within the bias range of ±0.2 V, which has been confirmed by STM characterization.[10,15] Figure 5i shows bias dependence of the edge state intensity observed in Figure 5a−h. The bias dependence of the edge state (*i.e.*, the suppression of the edge state intensity at the lower bias voltage) observed here suggests that oxidation can induce energy-dispersive character of the edge state, in which the DOS of the edge state is shifted away from the zero energy.

To understand (i) the spatially extended character and (ii) the energy-dispersive character of the edge state at the oxidized zigzag edge, electronic structure calculations based on DFT were performed using oxidized zigzag GNR models. From a theoretical point of view, formation energy of graphene edges terminated with hydroxyl, ether, carbonyl, and carboxyl functional groups can be defined in a system where bulk graphene is in equilibrium with carbon in its natural state and is in contact with a reservoir of foreign chemical species such as O_2 and H_2 molecules.[19−21] Recent theoretical calculations have predicted that zigzag edges terminated by hydroxyl,[19] carbonyl,[19−21] and carboxyl (lactone)[19] functional groups are stable with negative edge formation energy,[17,21] while positive free energy is found for ether terminations.[21] Actually, a previous XPS study demonstrated that hydroxyl, carbonyl, and carboxyl functional groups are formed by the electrochemical reactions.[26] In the present study, periodic LDOS modulations with a regular spacing of a (a = graphene lattice constant) were identified along the zigzag boundaries in the STM images (Figure 4b); therefore, zigzag edges regularly oxidized on the atomic scale in the forms C_{edge}−OH and C_{edge}=O groups were considered as model structures (C_{edge} = a carbon atom at the edge). We have not performed an exhaustive investigation of the various possible edge oxidation schemes, which remains to be investigated in a future study to clarify the detailed electronic properties of more complicated oxidized edge structures (*e.g.*, see Figure 2d).

Figure 6a,b shows band structures calculated on the basis of DFT with the local density approximation (LDA) functional for hydroxylated and ketonated zigzag GNR models.[18] The hydroxylated edge state could be identified by flat bands at E_f in a wave vector range $2/3\pi \leq k \leq \pi$, which is quite similar to the range of the hydrogenated zigzag edge.[8,9,15] In contrast, the ketonated zigzag edge featured a strongly modulated edge state with dispersive character (*i.e.*, metallic bands crossing E_f), and the edge state positions were within the wave vector range $0 \leq k \leq 2/3\pi$. The strong modulation might have originated from the unique participation of the additional π electron of the sp^2-hybridized oxygen atom in the graphene π electron system. Consequently, the boundary condition at the edge of the graphene π electron system changes from zigzag-type to bearded-type (known as a Klein edge).[30,31] The spatially localized edge state of the zigzag-type accordingly turns into an extended one, as has been

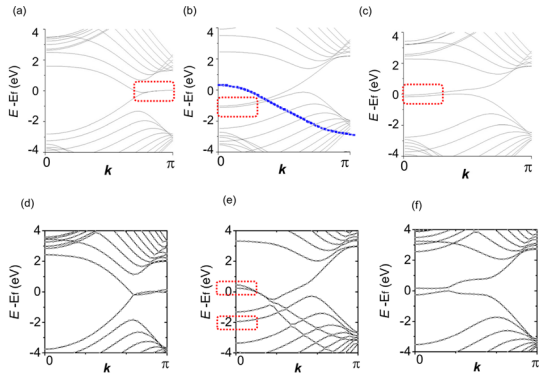

Figure 6. LDA−DFT calculated band structures of hydroxylated (a), ketonated (b), and Klein-type (c) (*i.e.*, dihydrogenated[15,30]) zigzag GNR models. Hybrid DFT calculated band structures of hydroxylated (d), ketonated (e), and Klein-type (f) zigzag GNR models. In (b), O-py lone-pair bands[18] are denoted by blue lines. Dotted red rectangles are visual guides provided to facilitate identification of the edge state. Nearly flat bands (*i.e.*, edge states) are visible in the wave vector range *ca.* $2/3 \leq k \leq \pi$ (a,d) and *ca.* $0 \leq k \leq 2/3\pi$ (b,c,f).

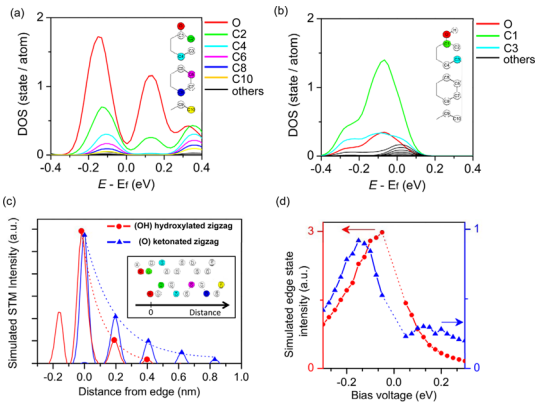

Figure 7. (a,b) Hybrid DFT calculated PDOS of the ketonated (a) and hydroxylated (b) zigzag GNR models. Inset: schematic models with the atom numbering. (c) Integrated PDOS from 0 to 0.3 V on each atom in the oxidized GNR models plotted as a function of distance from the edges (see models in the inset). The dotted curves in (c) indicate exponential curve fitting. (d) Simulated STM intensity of the edge atoms (*i.e.*, C2 for the ketonated GNR models and C1 for the hydroxylated GNR models) plotted as a function of V_{bias}. In both figures, blue triangles and red circles correspond to ketonated and hydroxylated GNR, respectively.

previously demonstrated in the one-orbital nearest-neighbor tight-binding approach.[32] Figure 6c shows the LDA−DFT calculated band structure of a bearded-type GNR model in which the edge state bands are at a wave vector range of *ca.* $0 \leq k \leq 2/3\pi$, which is similar to the range of the ketonated edge.

For the ketonated GNR, the LDA−DFT calculations of the edge state feature metallic bands crossing E_f;[18] a previous study has suggested that such calculations contain a self-interaction error that causes unphysical delocalization of the lone pairs in the edge oxygen atom.[20] Hybrid DFT reduces the self-interaction error by mixing in a fraction of the Hartree−Fock exchange into the exchange-correlation (XC) energy functional and significantly improves electronic properties such as band gaps.[33] A previous PBE0 DFT study has found that a zero band gap semiconducting property appeared in narrow ketonated GNR models with <1 nm width.[20] In this context, we adopted a hybrid DFT calculation with the PBE0 XC functional[34−36] using our relevant GNR model with a width of *ca.* 2.2 nm to determine the effect of the XC functional on the band structure. Figure 6d−f shows the calculated band structure for the hydroxylated (d), ketonated (e), and Klein-type (f) GNR models. The hybrid DFT calculation indicated that dispersion of the edge state bands for the hydroxylated and Klein-type model is almost the same as that obtained by the LDA−DFT calculation, whereas that for the ketonated model exhibits significant modification in which the edge state bands are split into two bands with a semimetallic nature (Figure 6e). Comparison of the band structures of the ketonated and the Klein-type edges (Figure 6e,f, respectively) suggested that additional charge transfer from the edge carbon atom to the oxygen atom with higher electronegativity in the ketonated edge[18] induces a significant dispersive character of the edge state.

Figure 7a,b shows the partial DOS (PDOS) calculated for the ketonated and hydroxylated zigzag GNR models. The PDOS of ketonated GNR indicates that the edge state (i) has a quasi-gap structure around E_f and (ii) decays into the bulk with finite amplitude at sites in one of the graphene sublattices (see C2, C4, C6, C8, and C10 sites in the structural model in Figure 7a). To simulate the STM current intensity (*i.e.*, edge state intensity) at $V_{bias} = 0.3$ V, the PDOS on each atom site was integrated from 0 to 0.3 V. The calculated edge state intensities on each atom were plotted against the corresponding distance from the edge boundaries (Figure 7c). The spatially localized and extended characters of the edge states are apparent in the hydroxylated and ketonated edges, respectively. The edge state intensity in the hydroxylated model decays within 0.4 nm from the edge boundary. On the other hand, the edge state intensity in the ketonated GNR model propagates into the bulk by more than 0.8 nm. The spatially extended character of the edge state in the ketonated GNR model is in good agreement with the experimental results (Figure 4b), in which the edge state extends up to *ca.* 1.5 nm into the bulk with finite amplitude on the edge oxygen atom and the interior carbon atoms on the same sublattice as the oxygen atom. To simulate the bias dependence of the edge state intensity (Figure 5i), the STM current intensity at the edge site (C2 atom in ketonated GNR and C1 atom in hydroxylated GNR) was calculated as a function of V_{bias} (Figure 7d). The best matching between theory and experiment was found for the ketonated zigzag GNR model, in which the energy-dispersive character with the unique quasi-gap structure is reproduced well. The oxidized zigzag edge with the modulated

edge state has been predicted to possess energetic stabilization[17] higher than that of the hydrogenated zigzag edge. This stabilization suggests that edge oxidation is important for the design of efficient and robust electronic/spintronic[17] devices.

CONCLUSIONS

We have successfully prepared nanosized graphene by fragmentation of the graphite surface in an electrochemical oxidation process. In addition to ragged graphene edges, atomically smooth zigzag edges were found on the periphery of the nanographene fragments. High-resolution STM characterization demonstrated that the edge state appearing at the atomically smooth zigzag edge of several nanometers was considerably different from that of the prototypical hydrogenated zigzag edge. The edge state in the oxidized zigzag edge was characterized by (i) an unconventional spatially extended character of up to 1.5 nm from the edge boundary and (ii) an energy-dispersive character with quasi-band-gap nature. DFT calculations indicated that the edge state could be modified by incorporation of oxygen π electrons into the graphene π electron system and by the charge transfer effect of the oxygen atom. The best match between the experimental results and DFT calculations was found for the ketonated zigzag edge, in which the participation of the oxygen π electron in the graphene π electron system results in strong modification of the boundary condition of the π electron network. The change in the boundary condition from zigzag-type to Klein-type caused the spatially extended character of the edge state. Such participation of the π electron cannot be expected for the sp^3-hybridized oxygen atom in the hydroxyl group. In general, graphene samples are usually in contact with air during preparation; therefore, oxidized structures are commonly present in real graphene materials. This study demonstrates that precise control over the oxidized structures is crucial for the emergence of the unique π state (edge state) in real graphene samples, which could be important in future graphene-based electronic/magnetic devices.

METHODS

Sample Preparation. Highly oriented pyrolytic graphite (HOPG, NT-MDT, GRHS grade, 3.5 ± 1.5° mosaic spread, 12 × 12 × 2 mm) was used as a working electrode. This was previously cleaved with adhesive tape to avoid surface damage to the basal plane. A HOPG surface of geometric area 0.6 cm^2 was mounted on the bottom of a Teflon three-electrode cell. A Pt plate counter electrode and Ag|AgCl|KCl (sat.) reference electrode were placed in the cell. The potential was measured against Ag|AgCl|KCl (sat.) (0.198 V *vs* SHE). The electrolyte solution was 0.1 M sulfuric acid. The electrochemical potential cycling tests were carried out in air by applying a triangular potential wave in the potential range of 0.8−1.7 V in 10 cycles at sweep rates of 20 $mV \cdot s^{-1}$. All electrochemical measurements were conducted at room temperature in aqueous H_2SO_4.

STM Characterization. STM experiments were performed using constant-current or constant-height modes using a commercially available STM system (Nano Scope III, Veeco) operating at room temperature in air. The tips used were composed of electropolished tungsten wire (Nilaco).

DFT Calculation. DFT electronic structure calculations were carried out using a plane-wave-based computational scheme as implemented in the Quantum ESPRESSO[37] or CASTEP[38] codes. We used the Perdew−Zunger functional (LDA)[39] and PBE0 hybrid functional.[34,35] The atomic positions were fully relaxed until the forces were less than 10^{-3} Ry/au. The DOS and band structure were investigated using moderately sized GNR models of approximately 2.2 nm width. In these calculations, combinations of ultrasoft[40] (norm-conserving[41]) pseudopotentials and plane-wave energy cutoffs of 400 eV (700 eV) were used for the LDA (PBE0) functional. For simulations of STM imaging within the Tersoff−Hamann approximation,[42,43] the wave function cutoff energy was set to 60 Ry (816 eV). The Brillouin zone integration was performed using a uniform 8 × 1 × 1 Monkhorst-type k-point grid.[44]

Conflict of Interest: The authors declare no competing financial interest.

Acknowledgment. This work was supported by Grants-in-Aid for Scientific Research (Nos. 20001006 and 23750150) from the Ministry of Education, Culture, Sports, Science and Technology of Japan.

Supporting Information Available: Converge tests of (i) PBE0-calclated total energy and band structure with respect to the wave function cutoff energy and (ii) band structure with respect to the ribbon width. This material is available free of charge *via* the Internet at http://pubs.acs.org.

REFERENCES AND NOTES

1. Novoselov, K. S.; Geim, A. K.; Morozov, S. V.; Jiang, D.; Zhang, Y.; Dubonos, S. V.; Grigorieva, I. V.; Firsov, A. A. Electric Field Effect in Atomically Thin Carbon Films. *Science* **2004**, *306*, 666–669.
2. Novoselov, K. S.; Jiang, Z.; Zhang, Y.; Morozov, S. V.; Stromer, H. L.; Zeitler, U.; Maan, J. C.; Boebinger, G. S.; Kim, P.; Geim, A. K. Room-Temperature Quantum Hall Effect in Graphene. *Science* **2007**, *315*, 1379.
3. Geim, A. K.; Novoselov, K. S. Role of Edges in the Electronic and Magnetic Structures of Nanographite. *Nat. Mater.* **2007**, *6*, 183–191.
4. Müllen, K.; Rabe, J. P. Nanographenes as Active Components of Single-Molecule Electronics and How a Scanning Tunneling Microscope Puts Them To Work. *Acc. Chem. Res.* **2008**, *41*, 511–520.
5. Enoki, T. Role of Edges in the Electronic and Magnetic Structures of Nanographite. *Phys. Scr.* **2012**, *146*, 014008.
6. Haddon, R. C. Graphene: Noble No More. *Acc. Chem. Res.* **2013**, *46*, 1–3.
7. Fujii, S.; Enoki, T. Nanographene and Graphene Edges: Electronic Structure and Nanofabrication. *Acc. Chem. Res.* **2012**, 10.1021/ar300120y.
8. Fujita, M.; Wakabayashi, K.; Nakada, K.; Kusakabe, K. Peculiar Localized State at Zigzag Graphite Edge. *J. Phys. Soc. Jpn.* **1996**, *65*, 1920–1923.
9. Nakada, K.; Fujita, M.; Dresselhaus, G.; Dresselhaus, M. S. Edge State in Graphene Ribbons: Nanometer Size Effect and Edge Shape Dependence. *Phys. Rev. B* **1996**, *54*, 17954–17961.
10. Kobayashi, Y.; Fukui, K.; Enoki, T.; Kusakabe, K.; Kaburagi, Y. Observation of Zigzag and Armchair Edges of Graphite Using Scanning Tunneling Microscopy and Spectroscopy. *Phys. Rev. B* **2005**, *71*, 193406.
11. Niimi, Y.; Matsui, T.; Kambara, H.; Tagami, K.; Tsukada, M.; Fukuyama, H. Scanning Tunneling Microscopy and

Spectroscopy Studies of Graphite Edges. *Appl. Surf. Sci.* **2005**, *241*, 43–48.
12. Pan, M.; Girao, E. C.; Jia, X.; Bhaviripudi, S.; Li, Q.; Kong, J.; Meunier, V.; Dresselhaus, M. S. Topographic and Spectroscopic Characterization of Electronic Edge States in CVD Grown Graphene Nanoribbons. *Nano Lett.* **2012**, *12*, 1928–1933.
13. Zhang, X.; Yazyev, O. V.; Feng, J.; Xie, L.; Tao, C.; Chen, Y.-C.; Jiao, L.; Pedramrazi, Z.; Zettl, A.; Louie, S. G.; *et al.* Experimentally Engineering the Edge Termination of Graphene Nanoribbons. *ACS Nano* **2013**, *7*, 198–202.
14. Talirz, L.; Söde, H.; Cai, J.; Ruffieux, P.; Blankenburg, S.; Jafaar, R.; Berger, R.; Feng, X.; Müllen, K.; Passerone, D.; *et al.* Termini of Bottom-Up Fabricated Graphene Nanoribbons. *J. Am. Chem. Soc.* **2013**, *135*, 2060–2063.
15. Ziatdinov, M.; Fujii, S.; Kusakabe, K.; Kiguchi, M.; Mori, T.; Enoki, T. Visualization of Electronic States on Atomically Smooth Graphitic Edges with Different Types of Hydrogen Termination. *Phys. Rev. B* **2013**, *87*, 115427.
16. Cervantes-Sodi, F.; Csányi, G.; Piscanec, S.; Ferrari, A. C. Edge-Functionalized and Substitutionally Doped Graphene Nanoribbons: Electronic and Spin Properties. *Phys. Rev. B* **2007**, *77*, 165427.
17. Hod, O.; Barone, V.; Peralta, J. E.; Scuseria, G. E. Enhanced Half-Metallicity in Edge-Oxidized Zigzag Graphene Nanoribbons. *Nano Lett.* **2007**, *7*, 2295–2299.
18. Lee, G.; Cho, K. Electronic Structures of Zigzag Graphene Nanoribbons with Edge Hydrogenation and Oxidation. *Phys. Rev. B* **2009**, *79*, 165440.
19. Zheng, H.; Duley, W. First-Principles Study of Edge Chemical Modifications in Graphene Nanodots. *Phys. Rev. B* **2009**, *78*, 045421.
20. Ramasubramaniam, A. Electronic Structure of Oxygen-Terminated Zigzag Graphene Nanoribbons: A Hybrid Density Functional Theory Study. *Phys. Rev. B* **2010**, *81*, 245413.
21. Seitsonen, A. P.; Saitta, A. M.; Wassmann, T.; Lazzeri, M.; Mauri, F. Structure and Stability of Graphene Nanoribbons in Oxygen, Carbon Dioxide, Water, and Ammonia. *Phys. Rev. B* **2010**, *82*, 115425.
22. Zhang, C. X.; He, C.; Xue, L.; Zhang, K. W.; Sun, L. Z.; Zhong, J. Transport Properties of Zigzag Graphene Nanoribbons with Oxygen Edge Decoration. *Org. Electron.* **2012**, *13*, 2494–2501.
23. Dreyer, D. R.; Park, S.; Bielawski, C. W.; Ruoff, R. S. The Chemistry of Graphene Oxide. *Chem. Soc. Rev.* **2010**, *39*, 228–240.
24. Weinberg, N. L.; Reddy, R. B. Electrochemical Oxidation of the Surface of Graphite Fibres. *J. Appl. Electrochem.* **1973**, *3*, 73–75.
25. Matsumoto, M.; Manako, T.; Imai, H. Electrochemical STM Investigation of Oxidative Corrosion of the Surface of Highly Oriented Pyrolytic Graphite. *J. Electrochem. Soc.* **2009**, *156*, B1208–B1211.
26. Choo, H.-S.; Kinumoto, T.; Nose, M.; Miyazaki, K.; Abe, T.; Ogumi, Z. Electrochemical Oxidation of Highly Oriented Pyrolytic Graphite during Potential Cycling in Sulfuric Acid Solution. *J. Power Sources* **2008**, *185*, 740–746.
27. Kuwabara, M.; Clarke, D. R.; Smith, D. A. Anomalous Superperiodicity in Scanning Tunneling Microscope Images of Graphite. *Appl. Phys. Lett.* **1990**, *56*, 2396–2398.
28. Macdonald, A. H.; Bistritzer, R. Graphene Moiré Mystery Solved? *Nature* **2011**, *474*, 453–454.
29. Jia, X.; Campos-Delgado, J.; Terrones, M.; Meunier, V.; Dresselhaus, M. S. Graphene Edges: A Review of Their Fabrication and Characterization. *Nanoscale* **2011**, *3*, 86–95.
30. Klein, D. J. Graphitic Polymer Strips with Edge States. *Chem. Phys. Lett.* **1994**, *217*, 261–265.
31. Kusakabe, K.; Maruyama, M. Magnetic Nanographite. *Phys. Rev. B* **2003**, *67*, 092406.
32. Son, Y.-W.; Park, N.; Han, S.; Yu, J. Magnetic Ordering at the Edges of Graphitic Fragments: Magnetic Tail Interactions between the Edge-Localized States. *Phys. Rev. B* **2005**, *72*, 174431.
33. Janesko, B. G.; Henderson, T. M.; Scuseria, G. E. Screened Hybrid Density Functionals for Solid-State Chemistry and Physic. *Phys. Chem. Chem. Phys.* **2009**, *11*, 443–454.
34. Perdew, J. P.; Ernzerhof, M.; Burke, K. Rationale for Mixing Exact Exchange with Density Functional Approximations. *J. Chem. Phys.* **1996**, *105*, 9982–9985.
35. Ernzerhof, M.; Scuseria, G. E. Assessment of the Perdew–Burke–Ernzerhof Exchange-Correlation Functional. *J. Chem. Phys.* **1999**, *110*, 5029–5036.
36. Adamo, C.; Barone, V. Toward Reliable Density Functional Methods without Adjustable Parameters: The PBE0 Model. *J. Chem. Phys.* **1999**, *110*, 6158–6170.
37. Giannozzi, P.; Paolo, G.; Stefano, B.; Nicola, B.; Matteo, C.; Roberto, C.; Carlo, C.; Davide, C.; Guido, L. C.; Matteo, C.; *et al.* QUANTUM ESPRESSO: A Modular and Open-Source Software Project for Quantum Simulations of Materials. *J. Phys.: Condens. Matter.* **2009**, *21*, 395502.
38. Clark, S. J.; Segall, M. D.; Pickard, C. J.; Hasnip, P. J.; Probert, M. I. J.; Refson, K.; Payne, M. C. First Principles Methods Using CASTEP. *Z. Kristallogr.* **2005**, *220*, 567–570.
39. Perdew, J. P.; Zunger, A. Self-Interaction Correction to Density-Functional Approximations for Many-Electron Systems. *Phys. Rev. B* **1981**, *23*, 5048–5079.
40. Vanderbilt, D. Soft Self-Consistent Pseudopotentials in a Generalized Eigenvalue Formalism. *Phys. Rev. B* **1990**, *41*, 7892–7895.
41. Lin, J. S.; Qteish, A.; Payne, M. C.; Heine, V. Optimized and Transferable Nonlocal Separable *Ab Initio* Pseudopotentials. *Phys. Rev. B* **1993**, *47*, 4174–4180.
42. Tersoff, J.; Hamann, D. R. Theory and Application for the Scanning Tunneling Microscope. *Phys. Rev. Lett.* **1983**, *50*, 1998–2001.
43. Tersoff, J.; Hamann, D. R. Theory of the Scanning Tunneling Microscope. *Phys. Rev. B* **1985**, *31*, 805–813.
44. Monkhorst, H. J. Special Points for Brillouin-Zone Integrations. *Phys. Rev. B* **1976**, *13*, 5188–5192.